AIChE

A Method to Calculate the Multiphase Flow Properties of Heterogeneous Porous Media by Using Network Simulations

Christos D. Tsakiroglou
Foundation for Research and Technology Hellas – Institute of Chemical Engineering and High Temperature Chemical Processes, Stadiou str., Platani, 26504 Patras, Greece

DOI 10.1002/aic.12493
Published online December 22, 2010 in Wiley Online Library (wileyonlinelibrary.com).

A method is suggested to compute the capillary pressure and relative permeability curves of heterogeneous porous media. The broad pore radius distribution (PRD) and throat radius distribution (TRD) are decomposed into relatively narrow component distribution functions which are used for the computer-aided construction of pore-and-throat networks. The quasi-static motion of menisci in pores and throats is tracked by accounting for capillary forces. The presence of fractal roughness along pore walls ensures the coexistence of both phases in pores. The calculation of the hydraulic conductance of each phase is based on the concept of constricted unit cell. Simulations in component pore networks constructed from narrow PRD and TRD produce a set of capillary pressure and relative permeability functions, the arithmetic averaging of which yields the corresponding functions for a heterogeneous synthetic pore network. This information is used by a dynamic simulator of drainage in permeability networks to predict experimental results of soil columns. © 2010 American Institute of Chemical Engineers *AIChE J,* 57: 2618–2628, 2011

Keywords: heterogeneous, porous media, pore network, simulation, relative permeability, capillary pressure

Introduction

More than 50 years after the pioneering work of Fatt,[1] the development of strong and fast computers has stimulated the widespread use of pore network models as advanced numerical tools that are capable to upscale efficiently the fluid-transport processes from the pore scale to the observation scale.[2,3]

A very wide variety of pore network approaches has been developed to simulate two-phase flow in porous media and reproduce the effective multiphase flow coefficients (e.g., capillary pressure curve, relative permeability functions, etc). In quasi-static mechanistic approaches, the multifluid displacement is governed by the capillary forces, the motion of menisci in pores follows rules of invasion percolation,[4] and fluid distribution is calculated at successive equilibrium states of drainage or imbibition cycles.[5-12] The oil/water drainage in a porous medium can be regarded as a gradient percolation process where the two-phase flow pattern is governed not only by capillary but also by gravity[13] and viscous[14] forces. Dynamic chamber-and-throat network simulators were first developed to account for the interactive effects of viscous and capillary forces on immiscible displacement processes and motion of ganglia in porous media by adopting the concept of elementary unit cells.[15,16] Later on, dynamic simulations in pore networks were used to track

This article is dedicated in the memory of Prof. Alkiviades Payatakes (deceased on November 29, 2009) whose pioneering work on the development of pore network simulators contributed substantially to the understanding of multiphase flow processes in porous media.

Correspondence concerning this article should be addressed to C. D. Tsakiroglou at ctsakir@iceht.forth.gr.

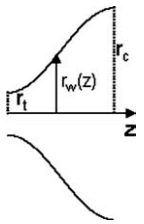

Figure 1. Elementary unit cell.

the transient evolution of parameters (e.g., pressure drop and saturation) during pressure-controlled or rate-controlled displacement processes and correlate the transient flow pattern with dimensionless pertinent parameters.[17-21] The simultaneous steady-flow of two phases through a porous medium has been simulated by dynamic network models based on either a mechanistic-type analysis[22] or a Lattice-Boltzman approach.[23] The roughness of natural porous media (e.g., sedimentary rocks and soils) has widely been modeled as a fractal surface to predict the finite hydraulic conductivity of the wetting fluid at low saturations.[24-26]

In the aforementioned studies, emphasis was placed on the calculation of the effective transport properties of reservoir rocks with application areas the enhanced oil recovery and subsurface contamination. However, during the last years, pore network models have been extended to simulate two-phase flow processes for a broad variety of applications like the water transport in the gas diffusion layer of polymer electrolyte membrane fuel cells,[27,28] the CO_2 sequestration in oceanic sediments,[29] or deep saline aquifers,[30] etc.

The three-dimensional (3-D) reconstruction of the pore-space with the aid of X-ray micro-CT scan tomography[31-35] and the simulation of multiphase flow in complex pore space morphologies with the aid of Lattice-Boltzman methods[36] has led to the development of advanced numerical methods for the calculation of the multiphase transport coefficients of 3-D porous media.[37]

Nevertheless, the simulation of multiphase flow in multi-scale pore networks with the pore sizes spanning several orders of magnitude is still a challenge. The pore structure analysis of soils[38] along with immiscible and miscible displacement experiments performed on undisturbed soil columns[39,40] revealed that the microporous matrix of mineral soils, composed of sand, clay, and silt is strongly heterogeneous, and the flow pattern is dominated by preferential flow paths. However, the capillary pressure and relative permeability curves at the mesoscopic scale (1–2 cm) of the soil column were produced implicitly with inverse modeling of the datasets of rate-controlled immiscible displacement experiments.[40] In this approach, any details of the pore structure were ignored, and the multiflow path model (MFPM), which is based on a simplifying representation of the porous medium, was used.[40] The effective two-phase flow coefficients were estimated through an iterative procedure, where the numerical solution of macroscopic mass and momentum balances (a system of ordinary differential equations) was fitted to experimental measurements.[40] However, having estimated the microscopic properties of the pore structure of the same soils,[38] it would be interesting to examine whether the effective two-phase flow coefficients could also be predicted by a bottom-up procedure of pore network modeling and compare the results of the two approaches.

To this goal, the broad pore radius distribution (PRD) and throat radius distribution (TRD) estimated by characterizing precisely the pore space of soils[38] are decomposed into several narrow component distribution functions. These component distribution functions are used for the computer-aided construction of Euclidean pore-and-throat networks with fractal roughness features superposed upon pore-walls. For the calculation of the hydraulic conductivity, the concept of the constricted unit cell of sinusoidal shape is adopted. The tortuosity of fractal roughness is specified by the length of the pore-wall curve. The quasi-static oil/water drainage in each network is simulated by tracking the motion of menisci according to the capillary resistance encountered in throats. The hydraulic conductivity or equivalently the relative permeability of each phase is calculated by imposing a pressure difference across it, "freezing" the other phase, formulating mass balances at each node (pore center), solving the system of linear equations, and determining the pressure field. The capillary pressure curve and oil/water relative permeability functions of the heterogeneous pore system are obtained with superposition of the corresponding simulated results of component pore networks, which are regarded as parallel conductors. Afterward, this information is fed into a dynamic simulator of the rate-controlled oil/water drainage in permeability networks to investigate the transient responses of the variables (fluid saturation and pressure drop) that are measured in soil column experiments.

Computer-Aided Construction of Pore-and-Throat Networks

The pore space is modeled as a 3-D network of "spherical" pores interconnected through "circular" and volumeless throats (primary porosity) with the roughness features (secondary porosity) regarded as cylindrical tubes superposed on the free surface of pores in cascade layers of self-similar structures. The PRD, TRD, and primary porosity (ε_p) are used as input parameters for the construction of the primary network, whereas the pore-wall roughness is modeled as a fractal surface (as it is described below) by using as parameters the ratio of secondary to total porosity, $A = \varepsilon_f/\varepsilon_t$, and fractal dimension D_s. These two parameters are obtained form the detailed characterization of the pore structure in terms of dual pore systems.[38,41] Two opposite sides of the network serve as entrance and exit, whereas periodicity is imposed along the rest boundaries. The parameters characterizing the reconstructed pore-and-throat networks are the following: (1) mean value, $\langle r_p \rangle$, and standard deviation, σ_p, of the PRD; (2) mean value, $\langle r_t \rangle$, and standard deviation, σ_t, of the TRD; (3) spatial pore-to-throat size-correlation coefficient, $\rho_{p\text{-}t}$, and pore-to-pore size-correlation coefficient, $\rho_{p\text{-}p}$; (4) absolute permeability, k, and electrical-formation factor, F.

Elementary unit cell and fractal roughness model

The concept of elementary unit cell is introduced to eliminate geometrical singularities when computing hydraulic and electrical conductances. A unit cell extends from the center of a throat to the center of its neighboring pore and has a sinusoidal geometry (Figure 1) described by the pore-wall function[15]

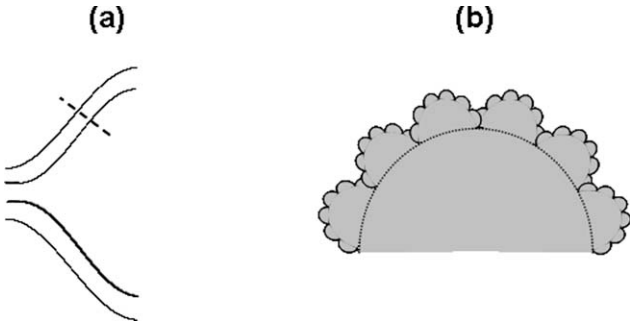

Figure 2. (a) Elementary unit cell surrounded by roughness features and (b) cross section of fractal roughness model.

$$r_w(z) = \frac{1}{2}\left[\left(r_p + r_t\right) - \left(r_p - r_t\right)\cos(2\pi z/l_c)\right] \quad (1)$$

where I_c is the length of periodicity, namely, the distance between the center of two adjacent pores. Roughness features (Figure 2b) are superposed upon each unit cell (Figure 2a). These features are regarded as bended cylindrical capillaries with a length

$$l_r = \int_0^{l_c/2} \sqrt{1 + \left(\frac{dr_w}{dz}\right)^2}\, dz = \sqrt{1+a^2}\,\frac{l_c E(k,\pi/2)}{\pi} \quad (2)$$

where $E(k,\pi/2)$ is an elliptic integral of second kind and parameters a,k are defined by

$$a = \frac{\pi\left(r_p - r_t\right)}{l_c} \quad (3)$$

and

$$k = \frac{a}{\sqrt{1+a^2}}, \quad (4)$$

respectively.

For the sake of consistency, it is assumed that the radii, r, of the roughness features of secondary porosity follow the distribution function

$$f_{s2}(r) = \frac{D_s r^{-(1+D_s)}}{r_{low}^{-D_s} - r_{up}^{-D_s}} \quad (5)$$

where the lower, r_{low}, and upper, r_{up}, cut-offs and surface fractal dimension, D_s, were obtained from the characterization of the pore structure of soils in terms of dual pore systems, by using an analogous fractal roughness model.[38] However, attempting to calculate explicitly the saturation and hydraulic conductance of each fluid, some additional approximations and assumptions are needed. For a unit cell (Figure 1), the upper cut-off is set equal to the average of throat and pore radii, namely

$$r_{up} = r_{av} = \left(r_p + r_t\right)/2 \quad (6)$$

The volume of roughness features belonging to the unit cell of pore i and throat j is given by

$$V_{r,ij} = l_r \int_{r_{low}}^{r_{up}} f_{s2}(r)\pi r^2 dr = \pi l_r \left(\frac{D_s}{D_s - 2}\right)\left(\frac{r_{low}^{2-D_s} - r_{up}^{2-D_s}}{r_{low}^{-D_s} - r_{up}^{-D_s}}\right) \quad (7)$$

and the sum of six (6) unit cells adjoining to pore i is given by

$$V_{r,i} = \sum_j V_{r,ij} \quad (8)$$

For all pores of the network, we have

$$V_{rt} = \sum_i V_{r,i} \quad (9)$$

and the normalization coefficient c_s is defined by

$$c_s = \frac{AV_{pt}}{(1-A)V_{rt}} \quad (10)$$

where V_{pt} is the total volume of primary porosity. For the sake of simplicity in the calculations of fluid saturation, each pore is represented by a spherical chamber resulting from the union of the adjacent elementary unit cells (Figure 3).

Modeling the Transport Properties of Pore Networks

Calculation of absolute permeability and formation factor

The calculation of the formation factor of pore-and-throat networks reduces to the analysis of electric circuits, whereas the absolute permeability is calculated by analogy to electric circuits. The pressure, the hydraulic conductance, and the volumetric flow rate are equivalent to the potential, the electrical conductance, and the current flow. Kirchoff's rules formulate that the sum of the voltages is zero for every closed loop of conductors and that the algebraic sum of the currents flowing into each node is also zero. From the application of these rules to the pore network, a system of coupled linear equations for the potential at each node is obtained. This system is solved using an iterative Gauss-Seidel method. Substituting the volumetric flow rate at the inlet of network and the pressure drop along it in Darcy's law, the absolute permeability is obtained.

The hydraulic, g_{huc}, and electrical, g_{euc}, conductance of a unit cell fully occupied by an aqueous solution of electrolyte are given by

$$g_{huc} = \frac{\pi}{8\mu_w l_c}\int_{z=0}^{z=l_c/2} r_w^4 dz \quad (11)$$

and

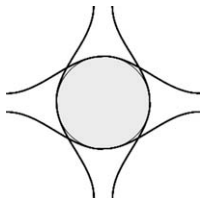

Figure 3. Elementary unit cells adjoining to a pore.

$$g_{euc} = \frac{\pi c_w}{l_c} \int_{z=0}^{z=l_c/2} r_w^2 dz, \quad (12)$$

respectively, where μ_w, c_w are the viscosity and specific electrical conductivity of the aqueous phase. The hydraulic, g_{hf}, and electrical, g_{ef}, conductance of the fractal roughness features superposed along a unit cell are approximated by

$$g_{hf} = \frac{\pi {r_{av}}^4}{8\mu_w l_r} \left[\frac{A^{(D_s-5)/(D_s-3)}}{1 - A^{(D_s-5)/(D_s-3)}} \right] \quad (13)$$

and

$$g_{ef} = \frac{\pi c_w {r_{av}}^2}{l_r} \left(\frac{A}{1-A} \right), \quad (14)$$

respectively. By regarding the primary unit cell and fractal roughness as two parallel resistors, the total hydraulic, g_{ht}, and electrical, g_{et}, conductance of the unit cell are given by

$$g_{ht} = g_{huc} + g_{hf} \quad (15)$$

$$g_{et} = g_{euc} + g_{ef} \quad (16)$$

Numerical simulation of oil/water drainage in water-wet networks

Drainage is a process where a nonwetting fluid displaces a wetting one at increasing values of the capillary pressure. At a current value of the external pressure, the pore network is scanned to search of throats that are accessible to the external oil sink and have size that allows a meniscus to penetrate into them. The critical capillary pressure for oil penetration into a throat of radius r_t is given by Washburn equation

$$P_c = \frac{2\gamma_{ow} \cos\theta_{ow}}{r_t} \quad (17)$$

where γ_{ow} and θ_{ow} are the oil/water interfacial tension and contact angle, respectively. Whenever $P_{ex} \geq P_c$, oil invades throat and adjoining pore, presuming that there is a noninterrupted column of water connecting it to the external water sink. Occasionally, blobs of trapped water may be created after the filling of a pore with oil. The procedure is repeated until no more menisci move, and capillary equilibrium is established. Then, a pressure difference is imposed across the network, and the Kirchoff's rules are applied separately to the equivalent electric subnetwork of each phase by "freezing" the other one. From the numerical solution of the resulting system of linear equations, the pressure at the center of each pore and the flow rate of the wetting and nonwetting phases at each unit cell is calculated. The inlet flow rates of water q_w and oil q_o along with the pressure drop across water, ΔP_w, and oil, ΔP_o, are introduced into the Darcy laws

$$\frac{q_w}{A} = \frac{k k_{rw}}{\mu_w} \left(\frac{\Delta P_w}{L} \right) \quad (18)$$

$$\frac{q_o}{A} = \frac{k k_{ro}}{\mu_o} \left(\frac{\Delta P_o}{L} \right) \quad (19)$$

to determine the water, k_{rw}, and oil, k_{ro}, relative permeability functions, where k, A, L are the permeability, cross-sectional area, and length of the pore network, respectively.

The assumptions that are adopted to simulate drainage in water-wet networks are summarized below.

a Water drains from a throat or pore only if there is a noninterrupted column of water connecting it to the external water sink.

b Water remaining along pore-wall roughness can drain unlimitedly and controls the hydraulic conductivity of wetting phase.

c Occasionally, blobs of water may be isolated in single pores or pore clusters surrounded by oil. Because of the very low-hydraulic conductance of the wetting films remaining in fractal roughness, the time spans required for water drainage from such pore systems, not connected to the water sink, may be very long. Under these conditions, and accounting for the finite equilibration times at each pressure value, it is assumed that the isolated blobs of water are trapped permanently.

d The pore network becomes hydraulically conductive to oil, soon after the breakthrough pressure, when a network spanning cluster of oil-occupied pores and throats is created for a first time.

e The hydraulic conductance of water remaining inside the fractal roughness features of a unit cell, after it has been invaded by oil, scales with the capillary pressure according to the relation[24-26]

$$g_w = g_{hf} \left(\frac{P_c r_{av}}{2\gamma_{ow} \cos\theta_{ow}} \right)^{D_s-5} \quad (20)$$

f The total hydraulic conductance of oil that has invaded a unit cell is given by the sum of two terms: (1) the hydraulic conductance of primary unit cell, Eq. 11, and (2) the hydraulic conductance of fractal roughness features occupied by oil. The second term is equal to the total hydraulic conductance of fractal roughness, Eq. 13, reduced by the conductance of roughness features occupied by water, Eq. 20, namely

$$g_o = \frac{\pi}{8\mu_o l_c} \int_{z=0}^{z=l_c/2} {r_w}^4 dz + \frac{\pi {r_{av}}^4}{8\mu_o l_r} \left[\frac{A^{(D_s-5)/(D_s-3)}}{1 - A^{(D_s-5)/(D_s-3)}} \right] \left[1 - \left(\frac{P_c r_{av}}{2\gamma_{ow} \cos\theta_{ow}} \right)^{D_s-5} \right] \quad (21)$$

The simulated capillary pressure curves of several realizations (with the network permeability k spanning some orders of magnitude) are fitted with the following models

$$P_{co} = c\gamma_{ow} \cos\theta_{ow} k^{-\delta} \quad (22)$$

$$(S_w - S_{wi}) \Big/ (1 - S_{wi}) = (P_c/P_{co})^{-1/m_c} - h_c \quad (23)$$

where P_c (S_w) is the capillary pressure function, P_{co} is the entry pressure, S_w is the water saturation, S_{wi} is the irreducible water saturation (at infinite P_c), and c, δ, m, h_c are parameters to estimate. The simulated water and oil relative permeability curves can be fitted with the following models

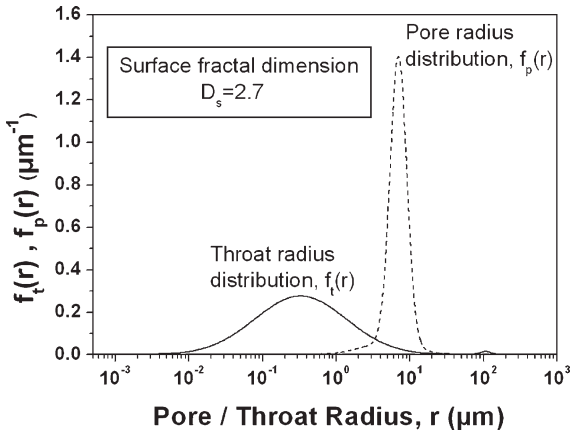

Figure 4. Pore radius distribution (PRD) and throat radius distribution (TRD) of a mineral soil sample (sample C7[38]).

$$\frac{k_{\mathrm{rw}}-k_{\mathrm{rwi}}}{1-k_{\mathrm{rwi}}}=a_{\mathrm{w}}\left(\frac{S_{\mathrm{w}}-S_{\mathrm{wi}}}{1-S_{\mathrm{wi}}}\right)^{e_{\mathrm{w1}}}+(1-a_{\mathrm{w}})\left(\frac{S_{\mathrm{w}}-S_{\mathrm{wi}}}{1-S_{\mathrm{wi}}}\right)^{e_{\mathrm{w2}}} \quad (24)$$

$$k_{\mathrm{ro}}=k_{\mathrm{ro}}^{0}\left[a_{\mathrm{o}}\left(\frac{S_{\mathrm{wc}}-S_{\mathrm{w}}}{S_{\mathrm{wc}}-S_{\mathrm{wi}}}\right)^{e_{\mathrm{o1}}}+(1-a_{\mathrm{o}})\left(\frac{S_{\mathrm{wc}}-S_{\mathrm{w}}}{S_{\mathrm{wc}}-S_{\mathrm{wi}}}\right)^{e_{\mathrm{o2}}}\right], \quad (25)$$

respectively, where k_{rwi}, a_{w}, e_{w1}, e_{w2}, S_{wc}, k_{ro}^{0}, a_{o}, e_{o1}, e_{o2} are parameters to estimate. The asymptotic water relative permeability $k_{\mathrm{rwi}} \geq 0$ corresponds to the irreducible water saturation $S_{\mathrm{w}} = S_{\mathrm{wi}}$ and is governed by the thickness of wetting fluid remaining along pore-wall roughness. The critical water saturation S_{we} corresponds to oil breakthrough ($k_{\mathrm{ro}} = 1$ if $S_{\mathrm{w}} \geq S_{\mathrm{wc}}$) and depends on the dimensions of pore network used in simulations. According to percolation theory, $S_{\mathrm{wc}} \rightarrow 1$ for an infinite network.[4]

Up-scaling the transport properties

A series of pore-structure characterization methods have recently been developed to probe pore sizes from several nanometers to several millimeters.[38,41,42] In this manner, the pore space of mineral soils and sedimentary rocks was analyzed in terms of the pore- and throat-size distributions of network models.[38] The autocorrelation function of back-scattered scanning electron microscope (BSEM) images was used to estimate the pore-size distribution over the range of large pore sizes, whereas high-pressure Hg intrusion data were used to extend the distribution to the range of small pore sizes. The experimentally measured Hg intrusion/retraction curves were introduced into inverse modeling algorithms to estimate the throat-size distribution along with the drainage and imbibition pore accessibility functions, which are related with the pore-space topology.[38,41] In the present work, the estimated PRD and TRD of the soil sample C7[38] are used as input data.

We are unable to construct a regular 3-D cubic network by respecting the multiscale heterogeneities expressed by the very broad pore- and throat-size distributions obtained (Figure 4). However, a set of homogeneous pore networks can be reconstructed by regarding the input pore- and throat-size distributions as subsets of the aforementioned complete distributions. The accurate approach requires that the subdivision of the complete distribution into component distributions, f_{pj}, obey the condition

$$f_{\mathrm{p}}(r)=\sum_{j=1}^{j=n}\beta_j f_{\mathrm{p}j}, j=1,2,\ldots,n \quad (26)$$

where β_j is the contribution fraction of component distribution $f_{\mathrm{p}j}$ to the overall one, f_{p}. Instead, the following semi-empirical procedure was followed. The lower, $r_{\mathrm{p}j,\min}$ and upper, $r_{\mathrm{p}j,\max}$, limit of the pore radii of $f_{\mathrm{p}j}$ are sampled randomly from the complete PRD $f_{\mathrm{p}}(r)$ (Figure 4), and the component network j is built by using the cumulative number-based fraction of pores, q_{sj}, defined by the relationship

$$q_{sj}=\int_{r_{\mathrm{p}j,\min}}^{r_{\mathrm{p}j,\max}} f_{\mathrm{p}}(r)dr \quad (27)$$

The lower, $r_{\mathrm{t}j,\min}$ and upper, $r_{\mathrm{t}j,\max}$, limit of the throat radii of the component distribution $f_{\mathrm{t}j}$, are so selected that the cumulative number-based fraction of throats (Figure 4) is equal to the corresponding fraction of pores, namely

$$q_{sj}=q_{\mathrm{b}j}=\int_{r_{\mathrm{t}j,\min}}^{r_{\mathrm{t}j,\max}} f_{\mathrm{t}}(r)dr \quad (28)$$

The ratio of the pore volume of the component network j to the total pore volume, $\varphi_{\mathrm{V}j}$, is defined by

$$\phi_{\mathrm{V}j}=\frac{\int_{r_{\mathrm{p}j,\min}}^{r_{\mathrm{p}j,\max}} r^3 f_{\mathrm{p}}(r)dr}{\int_{0}^{\infty} r^3 f_{\mathrm{p}}(r)dr} \quad (29)$$

and the contribution fraction, λ_j, of the component network j to the total porosity is defined as a weight fraction and obtained with normalization of the foregoing ratios, namely

$$\lambda_j=\frac{\phi_{\mathrm{V}j}}{\sum_j \phi_{\mathrm{V}j}} \quad (30)$$

In general, the averaging of the hydraulic and capillary properties of a heterogeneous porous medium composed of a system of homogeneous pore systems is based on a large-scale site percolation approach.[43] Here, a simplified approach is adopted where the heterogeneous pore structure is regarded as a system consisting of the component networks arranged in parallel each other (Figure 5). Assuming that the component networks do not interact, then the average permeability $\langle k \rangle$ and electrical formation factor $\langle F \rangle$ of the heterogeneous system are given by

$$\langle k \rangle=\sum_j \lambda_j k_j \quad (31)$$

and

$$\frac{1}{\langle F \rangle}=\sum_j \frac{\lambda_j}{F_j}, \quad (32)$$

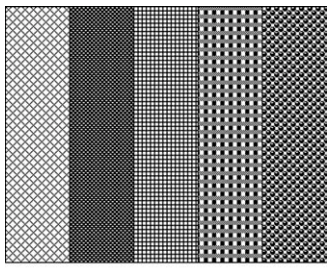

Figure 5. A synthetic pore network regarded as a system of parallel component networks.

respectively, where λ_j, k_j, F_j are the weight fraction, permeability, and formation factor of the component networks.

At a given capillary pressure, P_c, the water saturation of the component network j, S_{w_j}, is associated with water and oil relative permeability k_{rw_j} and k_{ro_j}, respectively. The corresponding average properties of the heterogeneous network are given by the relations

$$\langle S_w \rangle = \sum_j \lambda_j S_{w_j} \tag{33}$$

$$\langle k_{rw} \rangle = \frac{\sum_j \lambda_j k_{rw_j} k_j}{\langle k \rangle} \tag{34}$$

$$\langle k_{ro} \rangle = \frac{\sum_j \lambda_j k_{ro_j} k_j}{\langle k \rangle} \tag{35}$$

Large-Scale Dynamic Simulator in Permeability Networks

In general, the porous media may be heterogeneous at multiple length-scales.[38] Having incorporated all microscale heterogeneities into the average two-phase flow properties of the synthetic pore network (Figure 5), we need to describe the heterogeneity over a macroscopic length-scale. At a first approach, this macroheterogeneity could be described in terms of a distribution function of the permeability of synthetic pore networks. At the macroscale (soil column scale), the porous medium could be represented by a network of nodes of different permeability. Given that viscous forces become significant over large length-scales, the fluid-saturation distribution over the soil column scale can be predicted by using a dynamic simulator of the rate-controlled two-phase flow in permeability networks. Details of the simulator are reported elsewhere,[44] and its main steps are summarized below.

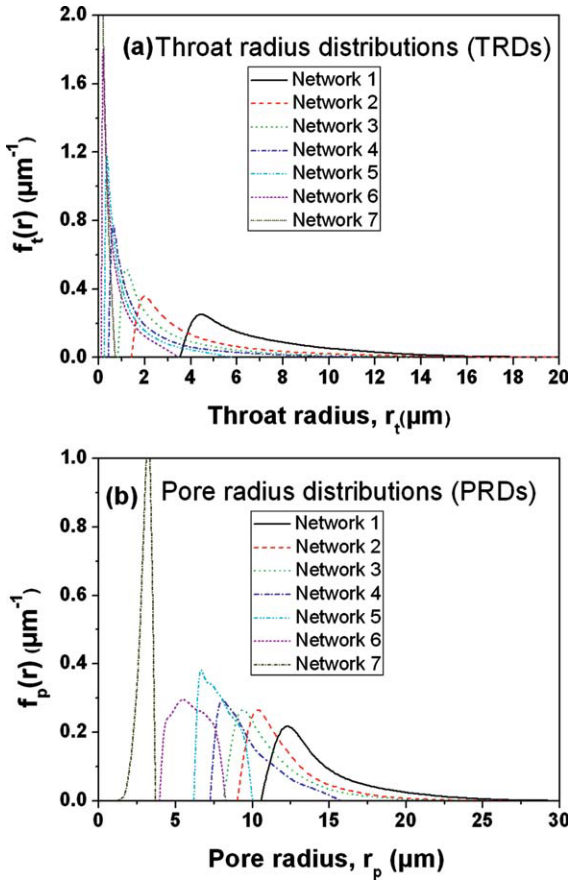

Figure 6. (a) Throat radius distributions (TRDs) of component networks and (b) pore radius distributions (PRDs) of component networks.

[Color figure can be viewed in the online issue, which is available at wileyonlinelibrary.com.]

The pore space is regarded as a cubic network consisting of nodes, each representing a pore network of varying permeability, chosen randomly or nonrandomly from a distribution function. The macroheterogeneity of the large network is quantified by the width of the node permeability distribution. In this work, the capillary pressure and relative permeability functions of nodes are set equal to those of the synthetic pore network and are assumed identical for all nodes. At each time step, the fluid saturation and pressure of each node are calculated by formulating mass balances at each node, accounting for capillary, viscous, and gravity forces, solving the system of linear and coupled equations, and calculating the instantaneous flow rates. At each

Table 1. Microscopic and Macroscopic Properties of Component Pore-and-Throat Networks

Network	$\langle r_p \rangle$ (μm)	σ_p (μm)	$\langle r_t \rangle$ (μm)	σ_t (μm)	$\rho_{p\text{-}t}$	$\rho_{p\text{-}p}$	k (mD)	F	λ_j
1	14.3	3.0	7.0	2.8	0.78	0.15	92.5	9.16	0.1932
2	12.0	2.4	4.3	2.9	0.63	0.05	20.1	13.8	0.1643
3	11.1	2.3	3.1	2.3	0.43	0.023	7.3	16.8	0.1654
4	9.8	1.8	2.1	1.9	0.23	0.022	2.3	19.6	0.1819
5	7.9	0.96	1.3	1.1	0.02	0.015	0.8	21.7	0.1428
6	6.0	1.08	0.8	0.68	0.005	0.009	0.26	23.3	0.0980
7	3.0	0.38	0.15	0.13	−0.011	0.058	0.004	28.1	0.0544

The equivalence, 1 mD = 10^{-15} m^2.

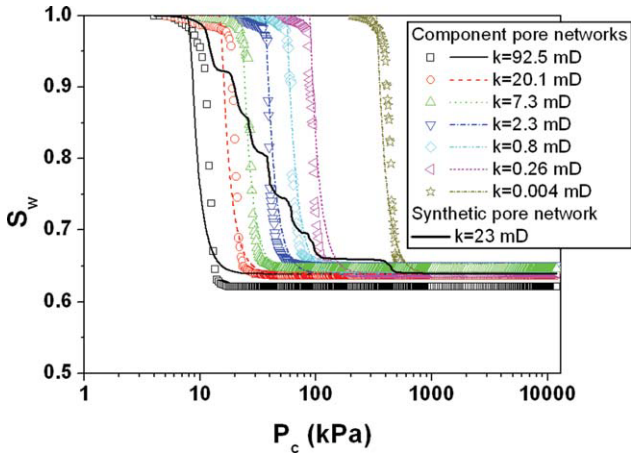

Figure 7. Simulated capillary pressure curves of component and synthetic pore networks.

[Color figure can be viewed in the online issue, which is available at wileyonlinelibrary.com.]

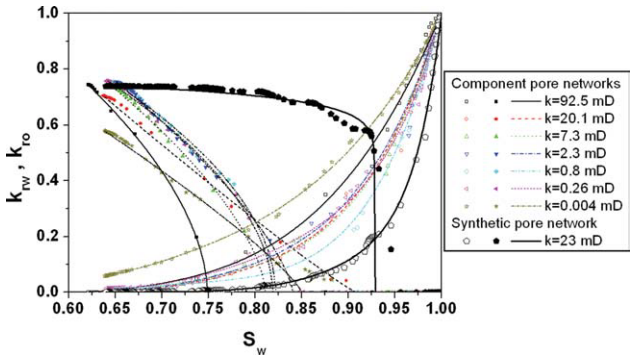

Figure 8. Oil and water relative permeability curves of component and synthetic pore networks.

[Color figure can be viewed in the online issue, which is available at wileyonlinelibrary.com.]

iteration of the algorithm, the pressure drop is so selected that the total flow rate of the injected fluid is kept constant.

The capillary pressure and relative permeability curves of the synthetic pore network may be evaluated by (1) comparing them with the corresponding two-phase flow functions estimated from flow tests on soil columns[40] and (2) predicting the macroscopic behavior of soil columns with the aid of the dynamic simulator of oil/water drainage in permeability networks, assuming that each node represents a synthetic pore network (Figure 5).

Results and Discussion

Capillary pressure and relative permeability curves

The pressure-controlled oil/water drainage was simulated in seven cubic pore-and-throat networks of dimensions 20 × 20 × 20 (number of nodes per axis) with the component PRD and TRD (Figure 6, Table 1) sampled from the complete ones (Figure 4). The simulated capillary pressure and relative permeability curves along with their best fits are shown in Figures 7 and 8, respectively, whereas the estimated parameter values of fitting functions are given in Table 2. According to Eq. 11, the hydraulic conductance of each unit cell scales as $g_{huc} \infty r_{av}^4$, where $r_t < r_{av} < r_p$. In this manner, the absolute permeability of component pore networks spans 5 orders of magnitude with the TRD and PRD spanning 2–3 and 1–2 orders of magnitude, respectively (Table 1). In spite of the account for the fractal roughness features along pore-walls in the calculations of saturation, the capillary pressure curves of component pore networks are narrow (Figure 7). In contrast, the capillary pressure curve of the (synthetic) system of parallel component networks is very wide (Figure 7) and representative of the broad range of pore-length scales probed (Figure 4). The stepping shape of P_c (S_w) is associated with the finite number of pore networks characterized by unimodal PRDs and TRDs (Figures 6a, b). The P_c (S_w) could be smoothed out if either the number of component networks was increased or the overlapping between PRDs and TRDs was enhanced.

When compared with the relative permeability curves of component pore networks, both the k_{rw} (S_w),k_{ro} (S_w) of the synthetic network shift to higher water saturations (Figure 8, Table 2). According to the critical path analysis of pore systems characterized by a broad range of pore throat sizes,[38,41,42] the hydraulic conductivity of each phase during drainage is governed by the permeability of the most permeable network spanning clusters of pores occupied by this phase. Given that in the heterogeneous synthetic pore network, oil starts occupying pores that are accessible through the largest throats, the oil relative permeability increases sharply as soon as a network spanning cluster of oil-occupied pores is established for a first time (Figure 8). Respectively, the water relative permeability decreases sharply, as soon as the continuity of the most permeable water-occupied critical path is interrupted, and gradually tends to very low but finite values because of the permanent presence of water film along pore-wall roughness (Figure 8).

Comparison of simulated with experimentally estimated results

The capillary pressure and relative permeability curves of the undisturbed soil column S3 (diameter D = 5 cm, length L = 32.7cm, porosity φ = 0.25, and permeability k = 50 mD) were estimated with inverse modeling of rate-controlled

Table 2. Parameters of the Fitting Functions of Relative Permeability Curves of Component Pore Networks

Network	k_{rwi}	a_w	e_{w1}	e_{w2}	k_{ro}^0	S_{wc}	e_o	S_{wi}
1	6.06×10^{-4}	0.2204	1.328	3.502	0.744	0.749	0.5603	0.6212
2	1.96×10^{-3}	0.3516	1.815	5.270	0.705	0.908	1.0816	0.6370
3	3.34×10^{-3}	0.2430	1.343	4.904	0.739	0.811	0.6253	0.6459
4	6.10×10^{-3}	0.3804	1.700	5.035	0.756	0.840	0.7000	0.6511
5	9.07×10^{-3}	0.0705	0.825	4.993	0.755	0.822	0.5232	0.6481
6	0.01398	0.5115	1.904	7.535	0.759	0.819	0.5361	0.6420
7	0.0583	0.4776	1.226	3.790	0.580	0.850	0.8300	0.6380

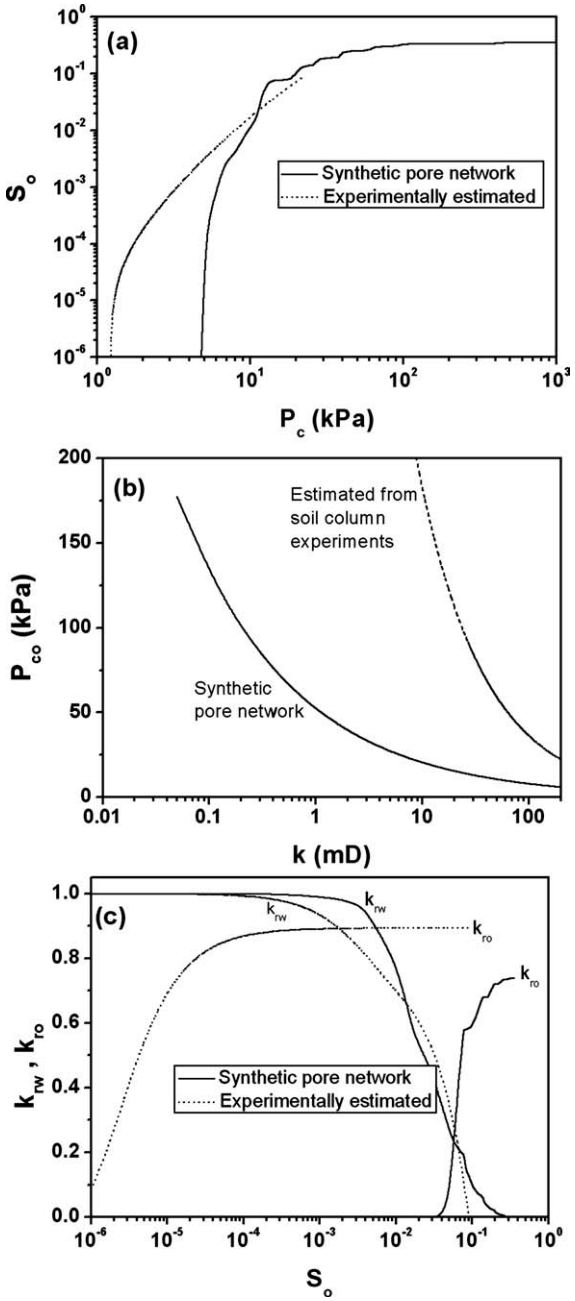

Figure 9. Comparison of network simulated with experimentally estimated (a) capillary pressure curve, (b) entry pressure as a function of permeability, and (c) water and oil relative permeability curves.

immiscible displacement experiments by using the MFPM.[38] The results obtained with inverse modeling are compared with the simulated ones in Figure 9. Instead of water saturation S_w, the oil saturation $S_o = 1 - S_w$ was used to emphasize the behavior of oil relative permeability over very low oil saturations (Figures 9a, c).

The P_c (S_o) estimated from flow tests with the MFPM is comparable with the simulated one, but shifts to lower pressures and extends over a narrow range of oil saturations because, under nonequilibrium conditions, oil flows through high-permeable preferential flowpaths and most of the water is bypassed (Figure 9a). On the other hand, the experimentally estimated entry capillary pressures are higher than those resulting from pore network simulations (Figure 9b) and this may be attributed to the different length scales: the simulated P_{co} (k) indicates the variation of P_{co} with the permeability of component pore networks (length scale $\sim 10^{-3}$ m); the P_{co} (k) of soil column quantifies the variation of P_{co} with the average permeability of the flowpaths (length scale $\sim 10^{-2}$ m), each comprising a different synthetic pore network (namely, system of parallel component pore networks).

Table 3. Parameters of Fitting Functions of P_c, k_{rw}, k_{ro} for the Synthetic Pore Network

Parameter	Estimated Value
m_c	0.1807 ± 0.0075
S_{wi}	$0.6388 \pm 9.75 \times 10^{-4}$
h_c	4.84×10^{-14}
c	0.8504 ± 0.043
δ	0.4057 ± 0.0015
k_{rwi}	$1.35 \times 10^{-3} \pm 7.5 \times 10^{-4}$
a_w	0.4056 ± 0.0462
e_{w1}	4.052 ± 0.287
e_{w2}	14.406 ± 0.962
e^0_{ro}	$0.742 \pm 2.6 \times 10^{-3}$
S_{wc}	$0.928 \pm 9.5 \times 10^{-4}$
e_o	$0.064 \pm 6.3 \times 10^{-3}$

The water relative permeability curves resulting from the two approaches are almost identical (Figure 9c) and their small differences can be attributed to the different boundary conditions (e.g., pressure controlled simulations vs. rate-controlled experiment). The k_{ro} (S_o) calculated with pore network simulations shifts to higher oil saturations compared with k_{ro} (S_o) estimated from soil column experiment (Figure 9c). This distance is associated with two factors: (1) the different scale of the synthetic pore network ($\sim 10^{-2}$ m) compared with that of the soil column ($\sim 10^{-1}$ m); (2) the equilibrium conditions prevailing in pore network simulations

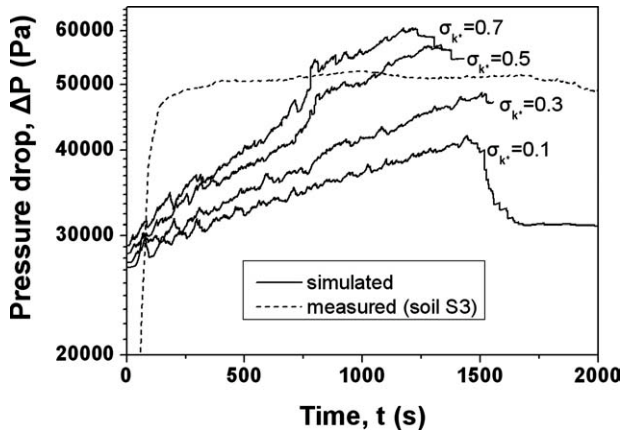

Figure 10. Simulated transient responses of the pressure drop across a heterogeneous permeability network for various values of the dimensionless standard deviation of the permeability distribution ($\langle k \rangle$ = 50 mD) are compared with corresponding experimental data of soil column S3.

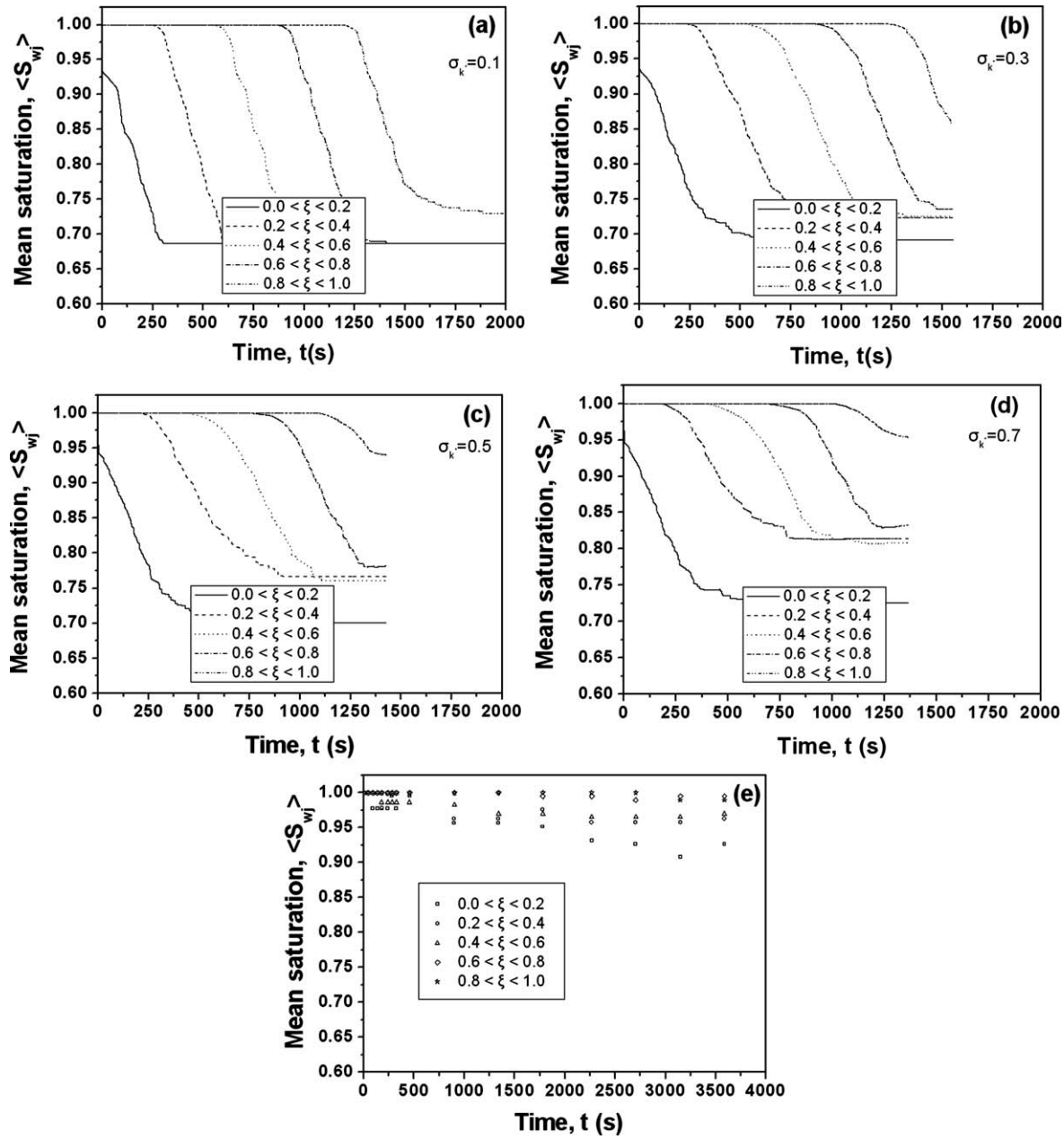

Figure 11. (a–d) Simulated transient responses of the axial water saturation profiles across a heterogeneous permeability network, for various values of the dimensionless standard deviation of the permeability distribution; (e) experimentally measured transient response of the axial water saturation profile across soil column S3.

The water saturation is averaged over five successive segments of the porous medium, $\langle S_{wj} \rangle$ ($j = 1, \ldots 5$) where index j denotes the segment, and ξ is the dimensionless axial distance from the porous medium inlet.

compared with the nonequilibrium displacement of water by oil during flow tests in soil columns. Nevertheless, a high end oil relative permeability, due to preferential flow paths, is estimated by both approaches (Figure 9c).

Dynamic simulation of oil/water drainage in permeability networks

The capillary pressure and relative permeability curves of synthetic network (Table 3) were fed as input data into the dynamic simulator of rate-controlled oil/water drainage in a cubic permeability network, where each node represents a synthetic network of varying permeability and identical P_c (S_w), k_{rw} (S_w), k_{ro} (S_w). The simulated transient responses of the pressure drop and axial distribution of water saturation across the network are sensitive to the width of node permeability distribution (Figures 10 and 11). The discrepancy between the simulated and experimental transient responses of $\Delta P(t)$ (Figure 10) may be attributed to the use of an underestimated P_{co} (k) in simulations compared with that estimated with inverse modeling (Figure 9b). On the other

hand, the differences between simulated (Figures 11a–d) and experimental (Figure 11e) responses of water saturations averaged over five successive segments, $\langle S_{wj} \rangle(t)$, may be ascribed to the use of an underestimated k_{ro} (S_o) in simulations compared with that estimated with inverse modeling (Figure 9c).

Perspectives for future work

Moreover, the foregoing two-step procedure suggested for the calculation of the properties of multiscale heterogeneous porous media could be improved by adopting the following modifications.

A more generalized approach might be required to determine the P_c, k_{rw}, k_{ro} functions of the synthetic pore network. Instead of the arithmetic averaging over a system of parallel networks, the synthetic pore network could be regarded as a random or spatially correlated cubic network of permeabilities, where each node is characterized by the P_c, k_{rw}, k_{ro} functions of the various component pore networks. Then, the oil/water drainage is modeled as a site percolation approach[43] and, in turn, these averaged P_c, k_{rw}, k_{ro} functions can be fed as input parameters into the dynamic simulator of drainage at the soil column scale.

The pore-scale heterogeneities probed at the scale of 1 cm may alter over the soil column scale, the TRD and PRD of the set of component pore networks may change, and therefore, the P_c, k_{rw}, k_{ro} functions of the corresponding synthetic networks may differ. Under such conditions, distributions rather than identical P_c, k_{rw}, k_{ro} functions should be fed as input parameters into the dynamic simulator.

Conclusions

A method was suggested to determine the capillary pressure and relative permeability functions of heterogeneous porous media from pore structure properties. Narrow TRDs and PRDs are properly sampled from the broad and complete ones, and used for the computer-aided construction of component pore-and-throat networks. Simulation of the quasi-static oil/water drainage in the component networks allows us to calculate the component capillary pressure and relative permeability functions. These functions are averaged arithmetically over a synthetic network composed of parallel component networks to estimate the capillary pressure and relative permeability curves of the heterogeneous medium. These P_c, k_{rw}, k_{ro} curves are fed as input parameters into a dynamic simulator of the rate-controlled oil/water drainage in permeability networks for calculating the transient responses of the axial distribution of water saturation, and pressure drop across the soil column-scale.

The very broad pore-length scales of a heterogeneous porous medium are reflected in a broad capillary pressure curve, whereas the sharp oil and water relative permeability curves are associated with the most permeable network spanning clusters of pores (preferential flow paths). Potential differences of calculated P_c, k_{rw}, k_{ro} from corresponding functions estimated with inverse modeling of experiments are interpreted in terms of differences with respect to boundary conditions and measurement length scale. A more generalized approach based on a large-scale site percolation model to calculate the averaged P_c, k_{rw}, k_{ro} functions of the synthetic pore network (1st step) along with the use of distributions rather than identical P_c, k_{rw}, k_{ro} functions in the dynamic simulator (2nd step) might improve both the P_c, k_{rw}, k_{ro} curves and prediction of the transient responses of the variables measured in immiscible displacement experiments.

Acknowledgments

This work was performed under Global Change and Ecosystems contract number SSPI-CT-2003-004017-STRESOIL (2004-2007) supported by the European Commission.

Literature Cited

1. Fatt I. The network model of porous media. I. Capillary pressure characteristics. *Pet Trans AIME*. 1956;207:144–159.
2. Dullien FAL. *Porous Media. Fluid Transport and Pore Structure, 2nd ed*. Oxford, UK: Academic Press, 1992.
3. Sahimi M. *Flow and Transport in Porous Media and Fractured Rock: From Classical Methods to Modern Approaches*. Weinheim: VCH, 1995.
4. Stauffer D, Aharony A. *Introduction to Percolation Theory*. London: Taylor & Francis, 1992.
5. Mani V, Mohanty KK. Effect of pore-space spatial correlations on two-phase flow in porous media. *J Pet Sci Eng*. 1999;23:173–188.
6. Knackstedt MA, Sheppard AP, Sahimi M. Pore network modelling of two-phase flow in porous rock: the effect of correlated heterogeneity. *Adv Water Resour*. 2001;24:257–277.
7. Laroche C, Vizika O. Two-phase flow properties prediction from small-scale data using pore-network modeling. *Transp Porous Media*. 2005;61:77–91.
8. Hou J. Network modeling of residual oil displacement after polymer flooding. *J Pet Sci Eng*. 2007;59:321–332.
9. Joekar-Niasar V, Hassanizadeh SM, Leijnse A. Insights into the relationships among capillary pressure, saturation, interfacial area and relative permeability using pore-network modeling. *Transp Porous Media*. 2008;74:201–219.
10. Chapuis O, Prat M, Quintard M, Chane-Kane E, Guillot O, Mayer N. Two-phase flow and evaporation in model fibrous media. Application to the gas diffusion layer of PEM fuel cells. *J Power Sources*. 2008;178:258–268.
11. Suicmez VS, Pri M, Blunt MJ. Effects of wettability and pore-level displacement on hydrocarbon trapping. *Adv Water Resour*. 2008;31:503–512.
12. Ryazanov AV, van Dijke MIJ, Sorbie KS. Two-phase pore-network modelling: existence of oil layers during water invasion. *Transp Porous Media*. 2009;80:79–99.
13. Houlin JP, Clement E, Baudet C. Quantitative analysis of an invading-fluid invasion front under gravity. *Phys Rev Lett*. 1988;61:333–336.
14. Xu B, Yortsos YC, Salin D. Invasion percolation with viscous forces. *Phys Rev E*. 1998;57:739–751.
15. Dias MM, Payatakes AC. Network models for two-phase flow in porous media. Part 1: immiscible displacement of non-wetting fluids. *J Fluid Mech*. 1986;164:305–336.
16. Dias MM, Payatakes AC. Network models for two-phase flow in porous media. Part 2: motion of oil ganglia. *J Fluid Mech*. 1986;164:337–358.
17. van der Marck SC, Matsuura, Glas J. Viscous and capillary pressures during drainage: network simulations and experiments. *Phys Rev E*. 1997;56:5675–5687.
18. Aker E, Maloy KJ, Hansen A. Simulating temporal evolution of pressure in two-phase flow in porous media. *Phys Rev E*. 1998;58:2217–2226.
19. Singh M, Mohanty KK. Dynamic modeling of drainage through three-dimensional porous media. *Chem Eng Sci*. 2003;58:1–18.
20. Nguyen VH, Sheppard AP, Knackstedt MA, Pinczewski WV. The effect of displacement rate on imbibition relative permeability and residual saturation. *J Pet Sci Eng*. 2006;52:54–70.

21. Bravo MC, Mariela Araujo M, Lago ME. Pore network modeling of two-phase flow in a liquid-(disconnected) gas system. *Physica A*. 2007;375:1–17.
22. Constantinides GN, Payatakes AC. Network simulation of steady-state two-phase flow in consolidated porous media. *AIChE J*. 1996;42:369–382.
23. Li H, Pan C, Miller CT. Pore-scale investigation of viscous coupling effects for two-phase flow in porous media. *Phys Rev E*. 2005;72:026705/1–026705/14.
24. de Gennes PG. *Partial filling of a fractal structure by a wetting fluid*. In: Adler D, Fritzsche H, Ovshinsky SR, editors. *Physics of Disordered Materials*. New York: Plenum Press, 1985:227–241.
25. Toledo PG, Novy RA, Davis HT, Scriven LE. Capillary pressure, water relative permeability, electrical conductivity and capillary dispersion coefficient of fractal porous media at low wetting phase saturation. *SPE Adv Technol Ser*. 1994;2:136–141.
26. Tsakiroglou CD, Fleury M. Pore network analysis of resistivity index for water-wet porous media. *Transp Porous Media*. 1999;35:89–128.
27. Markicevic B, Bazylak A, Djilali N. Determination of transport parameters for multiphase flow in porous gas diffusion electrodes using a capillary network model. *J Power Sources*. 2007;171:706–717.
28. Lee KJ, Nam JH, Kim CJ. Pore-network analysis of two-phase water transport in gas diffusion layers of polymer electrolyte membrane fuel cells. *Electrochim Acta*. 2009;54:1166–1176.
29. Kang Q, Tsimpanogiannis IN, Zhang D, Lichtner PC. Numerical modeling of pore-scale phenomena during CO2 sequestration in oceanic sediments. *Fuel Process Technol*. 2005;86:1647–1665.
30. Li L, Peters CA, Celia MA. Upscaling geochemical reaction rates using pore-scale network modeling. *Adv Water Resour*. 2006;29:1351–1370.
31. Ruiz de Argondona VG, Rodriguez Rey A, Celorio C, Suarez del rio LM, Calleja L, Llanova J. Characterization by computed X-ray tomography of the evolution of the pore structure of a dolomite rock during freeze-thaw cyclic tests. *Phys Chem Earth A*. 1999;24:633–637.
32. Santos LOE, Philippi PC, Damiani MC, Fernandes CP. Using three-dimensional reconstructed microstructures for predicting intrinsic permeability of reservoir rocks based on a Boolean lattice gas method. *J Pet Sci Eng*. 2002;35:109–124.
33. Al-Raoush RI, Wilson CS. Extraction of physically realistic pore network properties from three-dimensional synchrotron X-ray microtomography images of unconsolidated porous media systems. *J Hydrol*. 2005;300:44–64.
34. Appoloni CR, Fernandes CP, Rodrigues CRO. X-ray microtomography study of a sandstone reservoir rock. *Nucl Instrum Methods Phys Res A*. 2007;580:629–632.
35. Farber L, Tardos G, Michaels JN. Use of X-ray tomography to study the porosity and morphology of granules. *Powder Technol*. 2003;132:57–63.
36. Porter ML, Schaap MG, Wildenschild D. Lattice-Boltzmann simulations of the capillary pressure–saturation–interfacial area relationship for porous media. *Adv Water Resour*. 2009;32:1632–1640.
37. Ahrenholz B, Tolke J, Lehmann P, Peters A, Kaestner A, Krafczyk M, Durner W. Prediction of capillary hysteresis in a porous material using lattice-Boltzmann methods and comparison to experimental data and a morphological pore network model. *Adv Water Resour*. 2008;31:1151–1173.
38. Tsakiroglou CD, Ioannidis MA. Dual porosity modeling of the pore structure and transport properties of a contaminated soil. *Eur J Soil Sci*. 2008;59:744–761.
39. Aggelopoulos CA, Tsakiroglou CD. Quantifying soil heterogeneity from solute dispersion experiments. *Geoderma*. 2008;146:412–424.
40. Aggelopoulos CA, Tsakiroglou CD. A multi-flow path approach to model immiscible displacement in undisturbed heterogeneous soil columns. *J Contam Hydrol*. 2009;105:146–160.
41. Tsakiroglou CD, Ioannidis MA, Amirtharaj E, Vizika O. A new approach for the characterization of the pore structure of dual porosity rocks. *Chem Eng Sci*. 2009;64:847–859.
42. Amirtharaj ES, Ioannidis MA, Parker B, Tsakiroglou CD. Statistical synthesis of imaging and porosimetry data for the characterization of microstructure and transport properties of sandstones. *Transp Porous Media*. In press.
43. Yortsos YC, Satik C, Bacri J-C, Salin D. Large-scale percolation theory of drainage. *Transp Porous Media*. 1993;10:171–195.
44. Tsakiroglou CD, Sygouni V, Aggelopoulos CA. A dynamic network-type simulator to investigate the multiphase flow properties of heterogeneous soils. *Vadose Zone J*. 2010;9:285–294.

Manuscript received July 16, 2010, and revision received Sep. 17, 2010.